JCTC Journal of Chemical Theory and Computation

A Classical Potential to Model the Adsorption of Biological Molecules on Oxidized Titanium Surfaces

Julian Schneider*,† and Lucio Colombi Ciacchi†,‡

Hybrid Materials Interfaces Group, Faculty of Production Engineering and Bremen Center for Computational Materials Science, University of Bremen, D-28359 Bremen, Germany and Fraunhofer Institute for Manufacturing Technology and Applied Materials Research IFAM, D-28359 Bremen, Germany

Received August 6, 2010

Abstract: The behavior of titanium implants in physiological environments is governed by the thin oxide layer that forms spontaneously on the metal surface and mediates the interactions with adsorbate molecules. In order to study the adsorption of biomolecules on titanium in a realistic fashion, we first build up a model of an oxidized Ti surface in contact with liquid water by means of extensive first-principles molecular dynamics simulations. Taking the obtained structure as reference, we then develop a classical potential to model the Ti/TiO_x/water interface. This is based on the mapping with Coulomb and Lennard-Jones potentials of the adsorption energy landscape of single water and ammonia molecules on the rutile TiO_2(110) surface. The interactions with arbitrary organic molecules are obtained via standard combination rules to established biomolecular force fields. The transferability of our potential to the case of organic molecules adsorbing on the oxidized Ti surface is checked by comparing the classical potential energy surfaces of representative systems to quantum mechanical results at the level of density functional theory. Moreover, we calculate the heat of immersion of the TiO_2 rutile surface and the detachment force of a single tyrosine residue from steered molecular dynamics simulations, finding good agreement with experimental reference data in both cases. As a first application, we study the adsorption behavior of the Arg-Gly-Asp (RGD) peptide on the oxidized titanium surface, focusing particularly on the calculation of the free energy of desorption.

1. Introduction

The outstanding mechanical and chemical properties of titanium have attracted for decades the attention of materials scientists, leading to the development of Ti-based alloys for a broad range of applications. Besides its wide use in the aerospace and marine industries, its corrosion resistance and biocompatibility make titanium a material of choice for medical and dental implants.[1,2] In this case, a thorough knowledge of the physical and chemical details of the interface between the implant and the physiological environment is desired for tailoring the surface properties and optimizing the adhesion of cells within the body tissues. Since these processes are governed by the adsorption of biological macromolecules, such as proteins, an atomic-scale understanding of the interaction between proteins and the metal surface is often sought, yet still lacking.[3]

Complementary to experiments, atomistic molecular dynamics (MD) simulations, based on either quantum mechanical or classical formalisms, may provide a powerful method to gain insight into the microscopic mechanisms involved in protein adhesion. However, realistic simulations of the interface between titanium and a physiological environment have to face the rich chemical complexity of the system, which prevents the use of simple structural models and generic interaction potentials. In contact with water and oxygen, the metallic Ti surface is covered by an oxide layer, whose composition, structure, and thickness strongly depend on the oxidation conditions. It is known that high temper-

* Corresponding author. E-mail: schneider@hmi.uni-bremen.de.
† University of Bremen.
‡ Fraunhofer IFAM.

10.1021/ct1004388
Published on Web 12/23/2010

atures promote the formation of a thick TiO_2 layer, whereas oxidation at room temperature results in thin layers ($\leq$1 nm) composed of a broad range of titanium oxidation states and with stoichiometries variable from Ti_2O to TiO_2.[4−9]

When considering molecular adsorption on Ti surfaces, it is crucial to take into account the precise structure and chemistry of the oxide layer. In particular, since the oxidized Ti surface does not reveal single crystal features, it might be a too strong approximation to model it with an ideal TiO_2 crystal facet, as done so far in many simulation studies.[10−15] Recently, in extensive quantum mechanical MD simulations of the oxidation reactions of the bare metal, we have obtained a realistic model for the oxidized Ti(0001) surface, including two monolayers (ML) of chemisorbed oxygen atoms.[16] In agreement with the available experimental knowledge, this model reveals a rather amorphous oxide structure and variable Ti oxidation states and thus appears to capture well the representative features of Ti surfaces exposed to an oxidizing environment.

Although the adsorption reactions of small molecules, such as oxygen, can be simulated accurately by means of quantum mechanics,[11,17,18] the adsorption of large molecules over correspondingly extended surface areas can nowadays be investigated only by means of classical simulations. These require suitable 'force field' potentials to model the surface dynamics and the interactions between surface and adsorbate molecules. Several approaches are currently in use to model the interactions at the interfaces between titania and water or solvated organic molecules.[12,19,12] However, the current models are based on perfect crystal surfaces, and their transferability to thin oxide layers including various Ti oxidation states is uncertain. Furthermore, the available potentials have been scarcely validated for systems including more than 1 ML of water molecules, and the interactions with bulk water are rarely tested against suitable experimental results, such as the heat of immersion. Also the applicability of combination rules to extend the potentials to arbitrary molecules is often assumed but not investigated carefully.

As reported in ref 16, we have recently developed a force field to model the dry oxidized titanium surface in classical MD simulations. In this paper we present an extension of this force field to model Ti/TiO_x/water interfaces and in particular solvated organic adsorbate molecules interacting with oxidized Ti. The simple analytical form of our potential, based on atomic point charges and Lennard-Jones (LJ) interactions, is compatible with commonly used water models and biomolecular force fields and makes feasible the simulation of large systems. The potential parameters are accurately tuned on the basis of density functional theory (DFT) calculations of the potential energy surfaces (PES) of various organic molecules on the dry surface and validated against experimental results for the heat of immersion of TiO_2 as well as the adhesion force of tyrosine on oxidized Ti. As a first application, we present simulations of the adsorption behavior of the amino acid sequence Arg-Gly-Asp (RGD), which is widely used to functionalize biomaterials surfaces with the aim of promoting a better surface adhesion of cells in biomedical implants.

The paper is structured as follows: After a summary of the computational methods (Section 2), in Section 3 we describe first-principles molecular dynamics (FPMD) simulations of the interfaces between bulk water and both TiO_2 and the oxidized Ti(0001) surface. These calculations are used as a reference model for the construction of our potential in Section 4. In particular, we focus on an analysis of the charges of surface atoms and on how to achieve consistency with generic biomolecular force fields. We then proceed to derive appropriate nonbonded interactions and optimal parameters from DFT calculations of the PES of water and ammonia on the TiO_2 surface. In Section 4.4 we compare the classical model to DFT results of small organic molecules adsorbed on the dry oxidized surface. Subsequently, classical simulations of wet systems are presented and discussed in comparison to experimental results in Section 5. Finally, the adsorption behavior of the RGD peptide on the oxidized titanium surface is investigated in Section 6.

2. Computational Details

2.1. FPMD Simulations. Our FPMD simulations are performed within the formalism of DFT, employing the PW91 exchange correlation GGA functional[22] and the projector-augmented wave (PAW) method[23] to represent the interactions between electrons and core ions, as implemented in the Lautrec code.[24] The PAW data set for Ti is generated with 12 explicit valence electrons, including 3, 2, 2 projectors for the s, p, and d angular momentum channels. The data sets for O, N, and C include six, five, and four valence electrons and two projectors in each of the s and p channels. The wave functions are expanded in plane waves up to a kinetic energy cutoff of 540 eV. Since all systems under investigation are nonmagnetic, we employ spin-paired calculations. When considering metallic systems the electronic states are occupied according to a Fermi-Dirac distribution using a smearing width of 0.1 eV. Both the minimization of the electronic states and the MD simulations are performed using the Car−Parrinello (CP) method,[25] making use of special algorithms for the treatment of metallic systems[26,27] where necessary. The surface cells are sampled using the (0.25, 0.25) point of the Brillouin zone, except for the static PES calculations of water molecules on the TiO_2 surface (Section 3), where a 2×2 distribution is employed. For systems which bear an electric dipole moment (e.g., the dry oxidized surface), we apply an electrostatic correction to remove the macroscopic dipole along the z supercell direction.[28] In all geometry relaxations we ensure that all force components on all unconstrained atoms are less than 0.05 eV/Å. Convergence of total energy differences with respect to the chosen cutoff is checked in all cases to be within 0.01 eV.

2.2. Classical MD Simulations. All our classical MD simulations are performed using the program package DLPOLY[29] (version 3.09), in which we have implemented the force field for the dry oxidized surface. The electrostatic interactions are treated using the smoothed particle mesh Ewald (SPME) method with a precision of 10^{-6} and a real space cutoff of 12.0 Å. If not stated otherwise, for the short-

ranged interactions a cutoff radius of 12.0 Å is used. Dynamic simulations at finite temperature are performed in a NVT ensemble using the Berendsen thermostat[30] with a relaxation time of 0.5 ps and an integration time step of 1 fs. The surface slab is constructed by repeating the DFT dry surface cell structure in each direction of the surface plane and by applying a mirror operation along the perpendicular direction in order to obtain a symmetric system without net dipole moment. The resulting surface areas of the supercells comprise 17.62 × 20.34 $Å^2$ for the 2 × 2 surface and 35.23 × 40.68 $Å^2$ for the 4 × 4 surface. In dynamic simulations of the oxidized surface and the TiO_2 slab, the surface atoms are allowed to move according to the force field described in ref 16 (which is also reported in detail in the Supporting Information, for completeness). In Sections 5.2 and 6, the central plane of titanium atoms is fixed to provide a constant reference coordinate frame. Before adding any adsorbate molecules, the dry surface is relaxed classically. The surface water interface is prepared by filling the vacuum gap with pre-equilibrated water molecules. After relaxing and thermalizing the system in a 200 ps MD run, the height of the simulation cell is initially adjusted in another 100 ps simulation to obtain a 1 atm pressure along the surface normal. Prior to each production run, further equilibration simulations of at least 200 ps are carried out. Adsorbate molecules are prepared by relaxing their structure in vacuum and placing them in the dry simulation cell, which is then filled with pre-equilibrated water molecules. Subsequently the system is treated as described above.

3. FPMD Simulations of Water Adsorption

In order to obtain accurate model systems of the interfaces between oxidized titanium and bulk water, we perform extended FPMD simulations based on DFT, comparing the water adsorption behavior on a rutile(110) surface with that on an ultrathin oxide film grown on Ti (0001).[16]

3.1. Water Adsorption on Rutile TiO_2 (110). The dominant adsorption mode of water on the rutile TiO_2 (110) crystal surface has been the subject of controversial discussions for decades. Theoretical studies have reported contradicting energetic orders for either molecular, mixed, or dissociative adsorption at low water coverage (≤1 ML).[18,31,32] Regarding experimental results, spontaneous dissociation of water molecules on the perfect rutile(110) surface is generally considered to be unlikely, whereas it is facilitated at surface defect sites.[33−35] Recently, the change of free energy, rather than of potential energy, upon water adsorption was calculated in DFT MD simulations, yielding a positive value of +0.6 eV for the dissociation of bulk water on the perfect rutile(110) surface,[36] which corroborates the experimental finding. Here we consider a 4-layer slab of a 1 × 3 surface unit cell including 24 titanium and 48 oxygen atoms in contact with 21 water molecules. The dimensions of our supercell are 6.56 × 8.95 × 40.0 $Å^3$. By means of both dynamical simulations and static total energy calculations, we find that molecular adsorption at the five-fold-coordinated titanium atoms (Ti_{5f}) is the preferred way of interaction on the perfect TiO_2 rutile surface, in agreement with the Car−Parrinello MD studies of ref 31. In particular, when starting from an initially dissociated configuration with one of the protons bound to the neighbor bridging oxygen atoms, proton transfer and recombination of the water molecule eventually occurs within a few hundred fs of dynamics. Direct Ti−O bond formation between water and the surface takes place exclusively at Ti_{5f} atoms with a coverage close to 100%. Namely, all three equivalent Ti_{5f} sites of our surface cell remain occupied by an adsorbed molecule for more than 90% of the time during the FPMD simulations at ∼350 K.

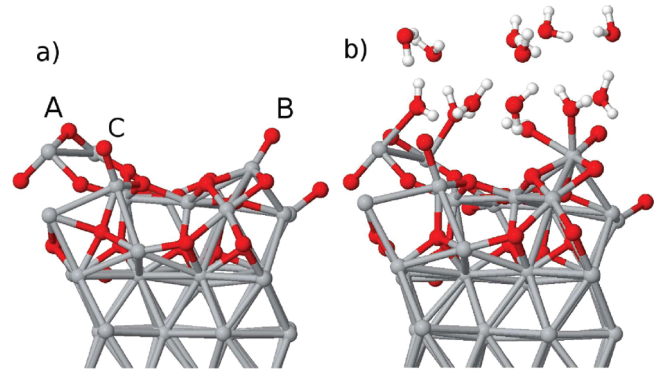

Figure 1. DFT model for the dry oxidized titanium surface (a) and snapshot of the interface between the surface and water from FPMD simulations (b).

3.2. Water Adsorption on Oxidized Ti(0001). A representative structural model for the oxidized Ti(0001) surface was obtained in extensive Car−Parrinello MD simulations, as described in ref 16 (Figure 1a). The model includes 60 titanium and 24 oxygen atoms corresponding to an O coverage of 2 ML. The structure of the oxide network exhibits a predominantly amorphous character, and its stoichiometry corresponds roughly to TiO, although features of different TiO_2 and Ti_2O_3 crystal structures can be identified.[16] As a remarkable topological property, the surface presents an exposed row of three two-fold-coordinated bridging oxygen atoms (labeled A, B, and C in Figure 1a), a typical feature observed on several TiO_2 crystal facets and on the oxidized TiN surface.[37]

Starting from this dry system we fill the vacuum gap with 28 pre-equilibrated water molecules and saturate the reactivity of the bottom surface of the slab with 12 hydrogen atoms in hcp positions, thus preventing spurious reactions between the water and the metallic slab. A FPMD simulation lasting 5 ps is carried out in the NVE ensemble, after initial thermalization of the system by velocity rescaling to a temperature of 350 K. During the dynamics, we observe adsorption, but not dissociation, of water molecules at exposed undercoordinated Ti atoms, similarly as on the rutile TiO_2(110) surface. In the case of the thin oxide film, the preferred adsorption sites are the Ti atoms which are bound to the two-fold-coordinated bridging oxygen atoms (which we will from now on refer to as TiB and OB, respectively). Once adsorbed, most of the molecules remain stably bound throughout the simulation. Only one molecule temporarily binds to a titanium atom located in the valley between the rows of bridging oxygen and later desorbs leaving the site free. In summary, a total of four water molecules stably adsorb on the surface during our FPMD trajectory, occupying three of the four TiB adsorption sites, one of which

accommodates two water molecules at the same time (Figure 1b). We calculate the desorption energies of these four water molecules from the total energy differences between the fully minimized water-decorated surface (in the absence of other free water molecules) and the same system upon removal of the adsorbed water molecules, one at a time, plus the total energy of the removed isolated water molecules in the same supercell. We obtain values of 0.53, 0.48, 0.91, and 0.44 eV. By comparison, for the desorption energy of a single water molecule from the fully hydrated 3 × 1 TiO_2(110) surface we find 0.83 eV.

In a further simulation, in which we started from a defective surface by removing one of the OB atoms, the adsorption of a water molecules takes place in a dissociative manner. One proton is transferred to a nearby bridging oxygen atom leaving a hydroxyl group adsorbed at the undercoordinated titanium atom. The corresponding calculated desorption energy value upon recombination of the dissociated molecule in the gas phase is 1.9 eV. Our computed values of desorption energy from the different sites agree fairly well with the values measured experimentally for the desorption of water from a ∼100 nm thick oxide layer on Ti.[38] Namely, two main desorption peaks at 0.53 and 0.75 eV were identified and assigned to desorption of molecularly adsorbed water on different surface sites, while a third peak at 1.2 eV was assigned to associative desorption from previously dissociated water molecules.

These results suggest that our model, although based on a system of very limited size, may indeed be representative of realistic Ti/TiO_x/water interfaces. We thus use it as a basis for constructing a classical potential which would enable us to simulate larger systems for longer time than achievable with a full quantum mechanical formalism. In doing this, we rely on the fact that our oxidized surface, in the absence of obvious defects, such as the oxygen vacancy that we arbitrarily created, showed little reactivity when exposed to liquid water. Therefore, we can assume that the physical/chemical behavior at the interface between oxidized Ti and the outer environment may be well captured by a simple potential based on nonbonded interactions, as described in the next section.

4. A Classical Potential for Ti/TiO_x/Water Interfaces

The starting point of our work is the classical force field potential which we have recently developed for the oxidized titanium surface. The model consists of a Finnis−Sinclair-type many-body potential for the metal region coupled to electrostatic Coulomb interactions and a short-ranged repulsive potential for the oxide region, as reported in the Supporting Information. In the next section, we focus on the coupling of this potential with a water environment and dissolved organic molecules, by combining it with standard molecular force fields.

4.1. Rescaling of the Point Charges for Surface/Adsorbate Interactions. In our potential, the point charges q_i employed in the electrostatic interactions within the oxide are determined using the electronegativity equalization method (EEM) of Mortier et al.[39] Their values within the thin oxide film (dashed line in Figure 2) are proportional to atomic Bader charges[40] computed at the DFT level and are consistent with the parametrization of the short-ranged interactions.[16] However, these charges are not guaranteed to reproduce well the electrostatic interactions between the oxide layer and the molecular species above the surface. Indeed, most common force fields for water or biomolecules, including the widely used TIP3P water model[41] or the AMBER[42] biomolecular force field, use point charges best fit to reproduce the electrostatic potential outside the molecule (ESP charges).[43−46] We thus compute ESP charges for the exposed OB and TiB atoms (for atoms buried in the surface, the ESP charge value has little or no significance). As shown in Figure 2, the obtained ESP charges are sightly lower than the EEM charges. Therefore, to compute the Coulomb electrostatic energy between molecular adsorbates and the oxidized surface, we rescale all surface point charges by a factor of 0.77, as determined ad hoc to match the EEM and ESP charges on the exposed surface bridging oxygen atoms (solid line in Figure 2). To calculate the interactions between the Ti and O atoms within the surface, we retain the original EEM charges in order to preserve the potential parametrization of ref 16.

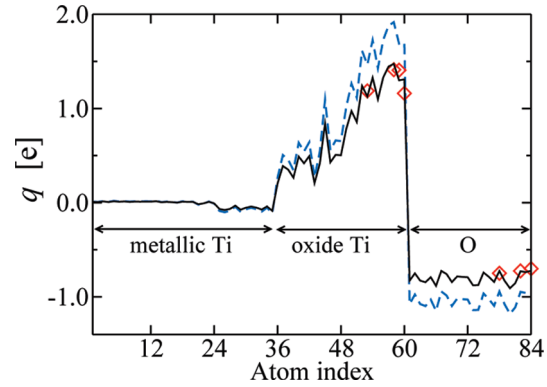

Figure 2. Charges of the dry oxidized titanium surface: Original EEM charges (dashed line, ---), scaled EEM charges (solid line, —), and the ESP charges of the exposed surface atoms (diamonds, ◊).

4.2. Interactions with Oxygen-Containing Molecules. The findings of Section 3, that water adsorption on the defect-free oxidized Ti surface takes place without dissociation, allow us to model the water/surface interactions by employing only electrostatic and nonbonded short-ranged forces. In this way, we can easily combine the potential described in the previous section with established biomolecular force fields in order to perform simulations of biomolecular adsorption on oxidized Ti, which is the ultimate goal of our work. We describe the interactions of the surface with adsorbates, in particular with water molecules, by a LJ and Coulomb nonbonded potential, as, e.g., in the AMBER force field:

$$V_{IJ}(r) = \varepsilon_{IJ}\left[\left(\frac{\sigma_{IJ}}{r}\right)^{12} - 2\left(\frac{\sigma_{IJ}}{r}\right)^{6}\right] + \frac{q_I q_J}{r} \qquad (1)$$

The parameters ε_{IJ} and σ_{IJ} for each pair IJ of interacting species can be obtained using the combination rules $\varepsilon_{IJ} = (\varepsilon_I \varepsilon_J)^{1/2}$ and $\sigma_{IJ} = (\sigma_I + \sigma_J)$.[42] The atomic parameters ε_I and

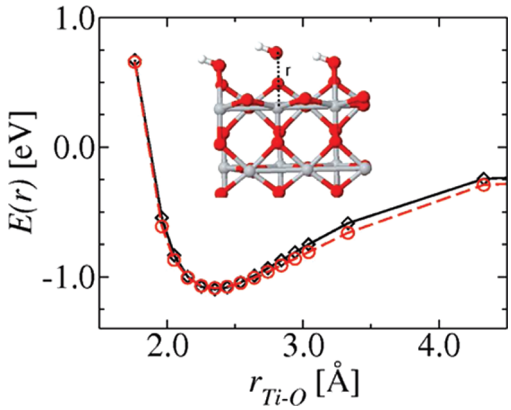

Figure 3. PES of a water molecule at various separations from the TiO_2 rutile(110) surface: DFT (black diamonds, ◊) and classical calculations (red circles, ○). The structure is displayed in the inset.

σ_I for water and biological molecules can be taken from the AMBER[42] or the generalized AMBER force field (GAFF),[47] which leaves only the four LJ parameters for the titanium and oxygen atoms of the surface to be determined. Differently from previous approaches (e.g., refs 20 and 21), we determine these parameters from a fit of the energy landscape of water desorbing from a rutile TiO_2(110) crystal surface, rather than from optimization of the structural properties of adsorbed water molecules.

As a reference, we compute with DFT the PES of one water molecule placed at different heights above the fully hydrated 3 × 1 rutile(110) surface cell, as displayed in the inset of Figure 3. Starting from a fully minimized configuration, one of the water molecules is displaced vertically along the surface normal, and total energy calculations are performed at each separation, keeping all atomic positions fixed. The resulting PES is shown in Figure 3 (black solid line), yielding a potential minimum of −1.1 eV. This is deeper than the desorption energy computed in Section 3 (0.83 eV) because of the lack of atomic relaxation.

For exactly the same atomic configurations, we now compute total energies using our classical potential, optimizing the LJ parameters for the surface atoms by a least-squares fit to the DFT PES using the GULP package.[48] Both the DFT and the classical energy values are rigidly shifted to obtain a value of 0.0 eV for a water surface separation of 8 Å. In these calculations, the point charges on the rutile atoms are computed from the EEM charges scaled by the same factor of 0.77 determined for the oxidized Ti surface (see previous section). Notably, the resulting charges are nearly identical to the ESP charges computed for the crystal surface (e.g., the average charge values of the bridging oxygen atoms are 0.67 electrons in both cases).

As shown in Figure 3, the agreement between the DFT and classical PES is excellent for the optimal LJ parameter set listed in Table 1. We note that in our approach the used LJ potential must not be seen as a physical representation of dispersion interactions but only as an arbitrary way of mapping the true surface water interactions by means of Coulomb and short-range terms. In fact, weak dispersion interactions are not properly accounted for, and generally underestimated,[49] in the DFT total energy calculations.

Table 1. LJ Parameters of the Surface Atoms

	LJ parameters	
	ε_I [eV]	σ_I [Å]
Ti	0.01455	0.7827
O	0.01983	1.6154
	Ti−N 9−6 potential	
ε_{Ti-N} [eV]	0.140155	
σ_{Ti-N} [Å]	2.30769	

Table 2. Interatomic Distances of the DFT and the Classical Model after Relaxation of the Water Molecules on the Rutile(110) Surface

	DFT	classical
Ti_5−OW [Å]	2.34	2.24
HW−OB [Å]	1.81	2.09
HW−OW [Å]	2.14	2.17

However, the deep minimum of the potential well on the polar oxide surface suggests that electrostatic attraction by far exceeds the dispersion forces, which can be thus safely neglected.

Using these interaction parameters, the water molecules are relaxed classically to compare the adsorbed geometry on the crystal surface to the corresponding DFT structure. Upon full atomic relaxation, at the classical level, the calculated desorption energies of a single water molecule from the hydrated surface is 0.81 eV, which is in very good agreement with the DFT value of 0.83 eV. We will indeed show later in the paper that these parameters lead to computed values of the work of hydration of Ti oxide surfaces in good agreement with experiments, thus justifying the approximations taken in our approach. The distances between five-fold titanium and water oxygen, between water hydrogen and bridging oxygen, as well as between hydrogen and oxygen of two neighbor water molecules are reported in Table 2. We notice small differences between the DFT and the classical structure, in particular the hydrogen bridges are longer in the classical model. However, we consider these differences as acceptable for our purposes, and we refrain from correcting them ad hoc by introducing bending potentials,[20,21] as they would prevent the desorption of the bound water molecules from the surface, or their replacement by other water molecules. These are events that we often observed in long FPMD simulations and that we would like to reproduce also in classical simulations.

Another feature which should be captured by the potential is the correct adsorption energy of a second water layer, as discussed in ref 21. To check this issue, we place an additional water molecule over the crystal surface terminated by three adsorbed water molecules, with the H atoms pointing toward the surface OB atoms. For this system we calculate the DFT and the classical PES as described above, obtaining adsorption energy minima of −0.14 and −0.12 eV for the DFT and the classical potential, respectively.

4.3. Interactions with Nitrogen-Containing Molecules. Obviously not all molecules of interest bind to the surface via oxygen atoms, as in the case of water. It is thus necessary

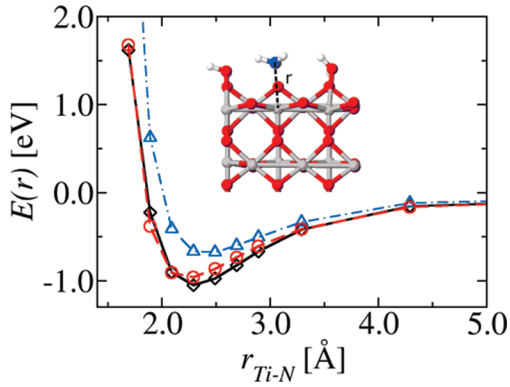

Figure 4. PES of an ammonia molecule at various separations from the TiO_2 rutile 110 surface: DFT (black diamonds, ◊) compared to classical calculations with original (blue triangles, △) and modified parameters (red circles, ○). The structure is displayed in the inset.

to check the transferability of the surface LJ parameters to the case of molecules adsorbing via different atoms, in particular nitrogen given its abundance in protein and other biomolecules. For this purpose we compute the adsorption of ammonia on the hydrated TiO_2(110) surface, as the simplest possible reference case. PES calculations are performed in the same way as described above, replacing only one of the water molecules by ammonia, while retaining the other two water molecules adsorbed on the surface. For the classical description of the NH_3 molecule, we use the LJ parameters taken from the GAFF. Since the AMBER force field does not specify partial charges for ammonia, we assign to the atoms ESP charges of −0.84 and +0.28, obtained by the same method as described in Section 4.1. Comparing the DFT and classical PES (Figure 4), it appears that the position of the energy minimum determining the equilibrium bond length is slightly shifted toward larger distances, and especially the depth of the potential minimum is too shallow in the classical case. Notably, even trying a further optimization of the LJ parameter of the surface Ti and O atom did not lead to satisfactory results. Depending on the particular circumstances, this deviation from the quantum mechanical behavior can be accepted either as a limit of the parameter transferability or a modification of the potential form must be introduced. In order to ensure a tight consistency with the DFT results, we chose to introduce an ad hoc 9-6 potential to model the interactions between N and Ti atoms:

$$V_{\mathrm{Ti-N}}(r) = \frac{\varepsilon_{\mathrm{Ti-N}}}{3}\left[6\left(\frac{\sigma_{\mathrm{Ti-N}}}{r}\right)^9 - 9\left(\frac{\sigma_{\mathrm{Ti-N}}}{r}\right)^6\right] \qquad (2)$$

The parameters $\varepsilon_{\mathrm{Ti-N}}$ and $\sigma_{\mathrm{Ti-N}}$ are determined by fitting to the DFT PES, the resulting values given in Table 1. With this potential form, the DFT adsorption energy profile can be now very well reproduced (Figure 4).

4.4. Adsorption of Organic Molecules on the Dry Oxidized Ti Surface. In this section, we check whether the force field parameters determined in the previous section taking the TiO_2(110) surface as a reference are transferable to the case of adsorption of small organic molecules on the oxidized Ti surface. To this aim, the PES of methanol (CH_3OH), formic acid (HCOOH), and methylamine (CH_3NH_2) above the dry oxidized titanium surface are calculated both by means of full-level DFT and of our newly developed classical potential. For the reasons mentioned in Section 4.3 and for the sake of consistency, for all molecules we computed ESP charges with our DFT code. These are found to differ by less than 0.05 e from the corresponding point charges of the AMBER force field, when available. The LJ parameters of all atomic pairs are obtained by the standard combination rules, as described above. For each of the molecules, the minimum-energy adsorption geometry is obtained by FPMD simulations followed by careful relaxation. Taking the resulting structures as the input models, the molecules are displaced along the directions of the bond connecting them to the surface, and total energy calculations are performed without atomic relaxation. The relaxed adsorbed configurations are shown in Figure 5.

In the case of formic acid, we found that the molecule could adsorb in either a molecular or a dissociated form, depending on the initial orientation of the carboxyl hydrogen. Since the dissociation reactions cannot be taken into account using our simple force field, we focus here on the molecularly adsorbed configuration. The OH group of methanol was found to bind to two titanium atoms, therefore the molecule was displaced vertically above the surface. Methylamine

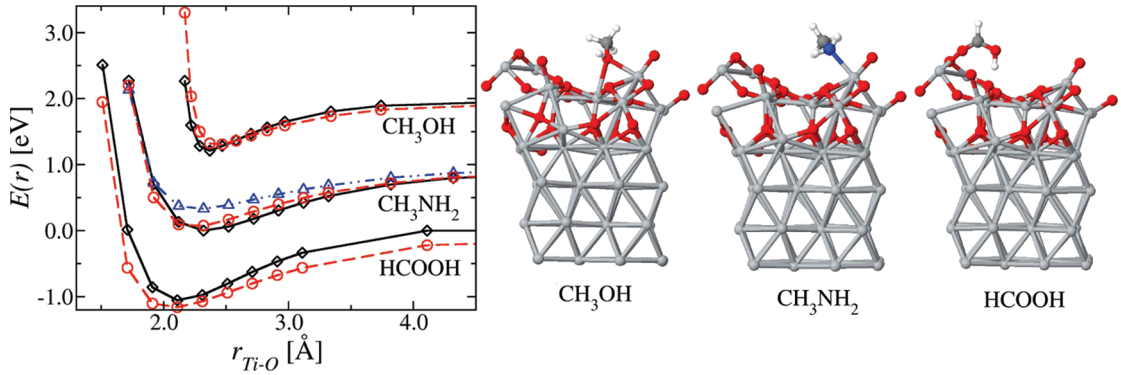

Figure 5. PES of methanol (CH_3OH), methylamine (CH_3NH_2) and formic acid (HCOOH) on the dry oxidized titanium surface: DFT (black diamonds, ◊) vs classical energies (red circles, ○). For CH_3NH_2 the results for unchanged (blue triangles, △) and modified (red circles) Ti−N interactions are displayed. For clarity the PES for CH_3NH_2 and CH_3OH are shifted vertically by 1.0, respectively, 2.0 eV.

adsorbs with the N atom of the amine group bound to a TiB atom of the surface.

For methanol, the PES obtained with our classical potential agrees very well with the energies calculated with DFT (Figure 5), in the case of formic acid the classical energies slightly overestimate the DFT values by about 0.1 eV. For methylamine, we find excellent agreement between the two PES when including the modified 9-6 Ti−N interaction potential, whereas using the standard 12-6 LJ potential for Ti−N results in considerably lower adsorption energy, although the equilibrium bond length is correctly reproduced.

5. Adsorption Behavior of Wet Systems

In the previous section, we have constructed a classical force field potential which is able to reproduce the adsorption energy of small molecules on both crystalline TiO_2 surfaces and thin oxide films grown on Ti(0001). Here, we apply our potential to investigate the behavior of interfaces between oxidized Ti and liquid water or fully solvated organic molecules. In particular, we take into account two representative cases for which quantitative experimental results are available, namely the heat of immersion of titanium oxide and the adsorption of single tyrosine molecules on oxidized Ti.

5.1. Heat of Immersion of TiO_x Surfaces. The heat of immersion of a surface, ΔH_{imm}, is defined as the energy gained upon placing the dry surface in contact with liquid water. In contrast to the case of, e.g., the oxidized silicon surface, where water molecules are stably chemisorbed in a dissociative manner, mostly molecular adsorption and physisorption of water takes place on titanium oxide surfaces, as already mentioned in Section 3. As found in TPD experiments, the desorption temperature of these molecules is around or even below room temperature.[34,38,50] Therefore, the amount of surface water molecules which remain bound to the surface upon drying cannot be unambiguously identified, as this significantly depends on the conditions of preparation, in particular on the drying temperature.[50] Correspondingly, as ΔH_{imm} depends on the number of molecules already bound to the surface prior to immersion in liquid water, scattered values between 0.2 and 0.6 J/m^2 have been reported for TiO_2 crystals.[50−52] A linear decrease of ΔH_{imm} with an increasing amount on initially adsorbed water on the TiO_2 rutile and anatase surfaces has been obtained in ref 50. Also in this study, however, the measured values scatter by as much as 0.3 J/m^2 for different investigated samples at the same initial water coverage, which makes possible only a rough comparison with theoretical investigations.

Here we start our study considering the interface between bulk water and a six-layer slab model of the rutile TiO_2(110) surface including a 6 × 12 surface unit cell comprising an area of 35.23 × 40.68 Å^2. Similar to what is observed in FPMD simulations, in classical MD runs at 300 K we observe water molecules binding preferentially to Ti_{5f} atoms, where they remained stably adsorbed for large part of the simulations. The heat of immersion can be calculated by subtracting from the average potential energy of the wet surface E_W the average potential energy of the corresponding dry surface E_D and the potential energy of bulk water containing the remaining number of water molecules E_B.[53] Starting from a 200 ps trajectory of the whole system with N_{tot} water molecules, these molecules are sorted with decreasing probability of being bound to the surface. The bulk water molecules are removed leaving only a certain number N_{ads} of molecules (according to their adsorption probability) on the surface. For these dry surfaces, simulation runs of 200 ps at a temperature of 300 K are performed to obtain the corresponding E_D average potential energies. From these values and the corresponding potential energy of bulk water containing $N_{tot} - N_{ads}$ water molecules, we calculate the heat of immersion as

$$\Delta H_{imm}(N_{ads}) = [E_D(N_{ads}) + E_B(N_{tot} - N_{ads}) - E_W(N_{tot})]/(2 * A_{Surf}) \quad (3)$$

where A_{Surf} is the surface area of only one side of the slab. The potential energies of the bulk water systems are calculated by first adjusting the height of each water cell in a 200 ps NPT run to obtain a pressure of 1 atm, followed by another 200 ps NVT simulation, in which the average energies were computed. A total number of 1188 water molecules is included as the liquid phase, and 'dry' surface systems with 24, 36, 64, 88, 120, and 144 preadsorbed water molecules are investigated. For N_{ads} = 144, all five-fold coordinated Ti atoms of the rutile 110 surface are occupied by water molecules.

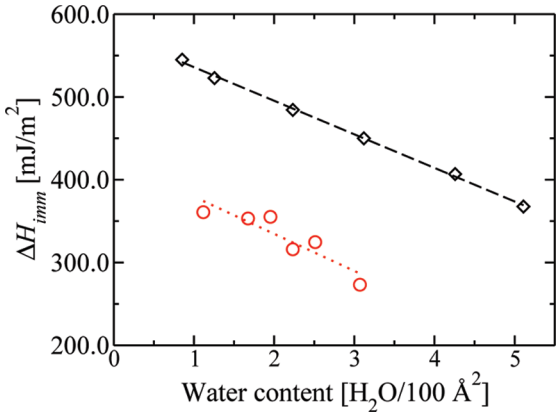

Figure 6. Heat of immersion for the TiO_2 rutile 110 surface (black diamonds, ◊) and the oxidized Ti surface (red circles, ○) as a function of the water content. The straight lines are linear fits to the data.

The resulting dependence of ΔH_{imm} on the number of preadsorbed water molecules is shown in Figure 6. In agreement with the findings of ref 50, a perfectly linear decrease is obtained, and also the absolute values compare well with those available in the literature (between 200 and 600 mJ/m^2, see above). The slope of the linear regression is 0.25 eV/H_2O, which represents the desorption energy per molecule from the surface into bulk water. If we neglect the hydration of adsorbed molecules, then the same quantity can be calculated by adding the heat of vaporization of water (−0.45 eV for TIP3P water)[41] to the desorption energy into the gas phase (∼0.8 eV, see above), obtaining 0.35 eV. A

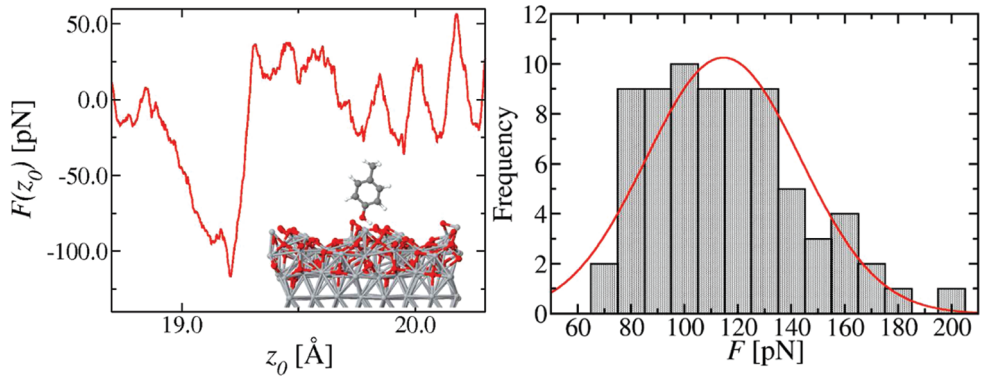

Figure 7. SMD simulations of tyrosine on the oxidized surface. Left: Example for a force−displacement curve $F(z_0)$. Right: Histogram of the maximum desorption forces and Gaussian fit to the distribution (red line).

comparison of these two numbers gives an estimate of about −0.1 eV for the hydration energy of adsorbed molecules on the surface.

We note that our value of 0.25 eV only takes into account molecular adsorption, while dissociative adsorption events on defective crystal sites, such as steps or edges, are expected to be associated with larger energy values (of the order of 1.2 to 1.9 eV, see Section 3). This may explain the significantly larger value of 0.82 eV/H_2O reported in ref 50 for the case of rutile powder samples.

The heat of immersion calculated for the oxidized surface displays a slightly different behavior. In this case, we include 1520 water molecules in the liquid phase in contact with the 4 × 4 repetition of the DFT surface model and performed 'dry' simulations for N_{ads} = 32, 48, 56, 64, 72, and 88. First of all, the obtained values are considerably lower than those for the crystal surface, as they range from about 260 to 380 mJ/m^2. They are closer to the value of 260 mJ/m^2 which has been reported for small TiO_2 nanoparticles.[51] Moreover, although a tendency of the heat of immersion to decrease upon increasing the preadsorbed water content can be identified, the values are scattered, and no clearly linear dependence is observed. This must be attributed to the fact that, in contrast to the perfect rutile surface, not all adsorption sites are equivalent on the oxidized surface, as indicated also by the scattered values of the static DFT adsorption energies on this surface (cf., Section 3). The scattering could possibly be reduced by changing the order of removing the water molecules and thus averaging over the different adsorption sites. However, sampling of a large number of permutations would increase the computer time exceedingly and lies beyond the scope of this work. Interestingly, fitting a linear function to the obtained values yields to a very similar slope compared to the crystal surface.

5.2. Desorption Force of Tyrosine. As a further validation of the force field, we calculate the maximum detachment force of single tyrosine residues from the oxidized titanium surface. This has been measured by AFM force spectroscopy experiments leading to a value of 97 ± 28 pN.[54] In our simulations, to exclude contributions from the backbone adsorbing to the surface, we consider a reduced molecule consisting of a phenol ring bound to a methyl group. The intramolecular interactions as well as the LJ parameters and the partial charges of the molecule are taken from the AMBER force field, and the charge value of the methyl carbon was adjusted to obtain a neutral molecule. After equilibration we then carry out a 39 ns classical MD run of the molecule on the oxidized surface at 300K, recording one snapshot every 500 ps. Seventy-eight of these snapshots were taken as independent starting configurations in subsequent umbrella-sampling runs. Such a large number of simulations yields reliable statistics for the force distribution, however, as a drawback, only the small 2 × 2 repetition of the DFT surface model could be used, to keep the computational cost reasonable. Due to the smaller cell size the cutoff radius for nonbonded interactions and for the real-space contribution of the electrostatic interactions had to be reduced to 8.0 Å.

Using a harmonic umbrella potential in the z direction normal to the surface applied to the carbon atom of the methyl group:

$$V_{umbr}(z_c) = \frac{1}{2}k_{umbr}(z_c - z_{umbr})^2 \quad (4)$$

with k_{umbr} = 0.2 eV/Å^2 and z_{umbr} = 16.0 Å (compared to $z \simeq 12$ Å for the exposed bridging oxygen atoms of the surface), the molecule was initially constrained to be close to the surface in a 300.0 ps simulation. In this representation, the z = 0.0 value refers to the central plane of titanium atoms, which are kept fixed. A steered molecular dynamics simulation (SMD) was then performed to mimic the experimental AFM setup, applying a time-dependent umbrella potential:

$$V_{smd}(z_c, t) = \frac{1}{2}k_{smd}(z_c - z_0(t))^2 \quad (5)$$

By choosing $z_0(t) = z_c(t = 0) + v_{smd} \cdot t$, the molecule is pulled off the surface at constant velocity. We set v_{smd} = 0.5 m/s and k_{smd} = 0.1 eV/Å^2. The instant pulling force $F(z_0) = k_{smd}(z_c - z_0)$ is recorded as a function of the pulling height z_0 every 5 fs. In order to eliminate large fluctuations, running averages of the force values over blocks comprising z_0 ranges of 0.025 Å are taken into account. In this way the short-time fluctuations are found to decrease considerably, whereas the actual force−displacement curve, which varies on a larger time scale, is not affected significantly.

A representative example of a force−displacement curve is shown in Figure 7. Initially the adhesion force increases roughly linearly until eventually a sudden decrease is visible,

which reflects the detachment of the molecule from the surface. We calculate the peak forces for a total number of 73 simulations, their distribution is displayed in a histogram in Figure 7. In five cases no clear force peak could be identified, indicating that the molecule was not adsorbed at the beginning of the simulations (more precisely, we did not consider peaks smaller than 60 pN, which corresponds to the fluctuations of the pulling force acting on a free, solvated molecule dragged through bulk water). These simulations were discarded and not considered in the histogram. Considering the trajectories of the individual simulations, we note that the adhesion to the surface is in general mediated by hydrogen bonds between the hydroxyl group of the phenol ring and the surface oxygen atoms, as assumed in ref 54. Moreover, in some cases the hydroxyl oxygen is observed to bind temporarily to one TiB atom after displacement of an adsorbed water molecule, leading to the values on the shoulder toward larger forces in the distribution. In summary, our computed forces range from 70 to 200 pN. A Gaussian distribution fit to the values yields an average force of 108 pN and a width of 31 pN. Within this variance the average force value agrees well with the experimental results of ref 54 (97 ± 28 pN). Therefore, we feel that our interaction potential can be reliably applied to investigate new systems, for which the experimental understanding is still incomplete, as performed in a representative case in the next section.

6. Adsorption of RGD Peptides on the Oxidized Ti Surface

Finally, as a first application of the developed force field, we present simulations of the RGD peptide sequence adsorbing on Ti. This sequence is present in proteins building the extracellular matrix, such as fibronectin and collagen, where it acts as an integrin binding site and plays an important role in the process of cell adhesion.[55] Since such peptides are used to functionalize the surfaces of metal implants to enhance bone cell adhesion,[56,57] an interesting aspect is their direct adsorption behavior, as this competes to binding to integrins. Despite its importance, only a few simulation studies are devoted to the investigation of the adsorption of RGD sequences on solid-state surfaces, particularly on crystalline titanium oxide.[14,15,58]

Here we perform umbrella sampling simulations to obtain force−displacement profiles from which the potential of mean force (PMF) and the free energy of adsorption can be calculated. In order to avoid charged end groups, the molecule is terminated with NME (CH_3NH-) and ACE ($-COCH_3$) sequences, yielding a NME-Asp-Gly-Arg-ACE peptide. The peptide is completely modeled using the AMBER force field, including its partial charges. For similar reasons as stated in Section 5.2, we consider a 2 × 2 surface area and use a cutoff radius of 8.0 Å. After pre-equilibrating and adjusting the cell height, the system is annealed at 450 K for 200 ps (keeping the surface atoms fixed) to overcome possible adsorption barriers to the surface, followed by another annealing at 300 K for 300 ps. The resulting configuration, which is shown in Figure 8c, is used as initial model for our free energy calculations.

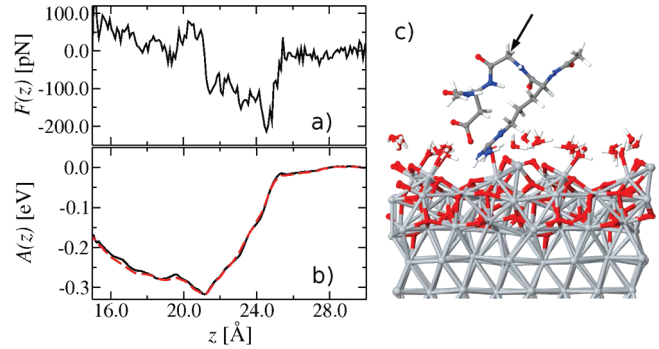

Figure 8. Desorption of the RGD-containing peptide from the oxidized Ti surface: Force profile (a), free energy profile obtained by WHAM (solid line) and TI (dashed line), and snapshot of the initial adsorbed configuration (c). For clarity, only the first layer of water molecules is displayed. The arrow marks the Gly α-carbon atom.

The RGD molecule binds to the surface via the Arg side chain, which is able to penetrate the first layer of water molecules in the valley between two rows of bridging oxygen atoms. The interaction with the surface is mediated both via hydrogen bonds between the guanidine group and surface oxygen atoms and via electrostatic interactions between nitrogen and titanium atoms. The ASP side chain is also oriented toward the surface, with the carboxyl oxygen atoms forming hydrogen bonds with the Arg side chain and with surface water molecules.

In the umbrella sampling simulations, as the reaction coordinate we chose the z-position $z_{c\alpha}$ of the α carbon of the central Gly residue, with a zero offset corresponding to the position of the central plane of the surface slab (as described in Section 5.2). The reaction coordinate is then increased stepwise from 16.0 to 29.0 Å and restrained to a total of 14 windows with 1.0 Å width by a harmonic potential (see Section 4) with a force constant $k_{umbr} = 0.2$ eV/Å^2. For each window a simulation run of 1.2 ns is performed, where the first 200 ps are discarded from the force analysis. The reaction coordinate and the z-component of the force acting on it are recorded every 5 fs.

To calculate the free energy profile $A(z)$, we employ two conceptually different methods, namely: (i) the weighted histogram analysis method (WHAM),[59] evaluating the probability using the code of Grossfield,[60] and (ii) the PMF as obtained by thermodynamic integration (TI) of the average force:[61,62]

$$A(z) = -\int_{z_{max}}^{z} \langle F(z')\rangle dz' \qquad (6)$$

The unbiased force is obtained by performing the average over all umbrella windows and correcting the value by the respective umbrella force:

$$\langle F(z)\rangle = \sum_{i=1}^{N_{umbr}} \frac{n_i(z)[\langle F^i_{biased}(z)\rangle + (dV^i_{umbr}(z)/dz)]}{n_{tot}(z)} \qquad (7)$$

where the i indicates the respective umbrella window, $n_i(z)$ gives the number of appearances of a reaction coordinate value of z from umbrella window i, and $n_{tot}(z) = \sum_i n_i(z)$

yields the total number of counts for the value z. The forces, probability, and corresponding free energy profile are collected in bins of 0.1 Å width.

The unbiased force profile $F(z)$ is displayed in Figure 8a. When increasing the z_0 value of the umbrella center, first the side chain of the Asp residue is detached from the surface due to its shorter length compared to Arg. Finally the guanidine group of the Arg residue desorbs producing a force peak of about −215 pN at a z-value of 24.5 Å in the force profile. The free energy profiles calculated with the two methods are shown in Figure 8b. Importantly, we note that the two curves agree almost perfectly with each other, giving a strong hint that the force calculations and the reaction coordinate sampling have reached convergence. In the free energy profile we observe a minimum depth of 0.32 eV, which can be interpreted as the free energy of desorption. Experimental values for the binding free energy between RGD-containing peptides and integrin proteins in the absence of a surface are found to be in the range of 0.16 eV,[63] whereas simulations of such a situation yield a binding free energy of 0.13 eV.[64] Hence, when a titanium surface is functionalized using RGD-containing peptides, a situation might arise where adsorption on the surface is in competition with the desired process of binding to integrin molecules. From a comparison of the respective free energy values we can conclude that the adsorption of RGD on the oxidized titanium surface is considerably stronger and might thus limit the functionality of the sequence. Therefore, covalent biding via appropriate spacers, where direct adsorption of RGD at the titanium surface is avoided, should be preferred over nonspecific surface adsorption to enhance cell adhesion via binding to integrin.

7. Conclusions

In summary, we have presented an extension of the classical force field developed in ref 16 to model the interactions between natively oxidized titanium surfaces and liquid water as well as solvated biomolecules. The interactions across the solid/liquid interfaces comprise Coulomb forces between ESP point charges and a L J potential, whose coefficients for the surface atoms have been determined by fitting the classical PES of a water molecule at various separations from the TiO_2 rutile 110 surface to the corresponding DFT energies. In this way, the potential is fully consistent with commonly used biomolecular force fields. We have demonstrated that the interactions with generic organic molecules can be reliably obtained by applying standard combination rules to the GAFF. In particular, the obtained potential is fully transferable to the case of molecules containing O, C, and H atoms adsorbed on thin oxide layers grown on metallic Ti, for which the adsorption PES calculated with full DFT and with our classical potential is excellent. However, if the direct surface-molecule interactions involve nitrogen atoms, quantitative agreement between the DFT and classical PES could be obtained only after introducing an additional 9-6 potential to model the Ti−N interactions. After adjusting the respective potential parameters, using an NH_3 molecule adsorbed on the partially wet rutile surface as a reference, excellent transferability to the case of the natively oxidized surface has been found.

As mentioned before, the major approximation intrinsic in our potential parametrization is the use of standard DFT calculations to determine the reference surface/molecule interactions, which do not properly take into account dispersion forces. If necessary, more sophisticated methods to compute the reference PES should be employed, and the LJ parameters of the interaction potentials correspondingly adjusted, while the chosen analytic form of the potential certainly allows for dispersion forces to be described correctly. However, in our specific case where highly polar surfaces are considered, the electrostatic contributions far exceed weak forces of the van der Waals type, resulting in adsorption energies of the order of 0.8 eV per water molecule. Indeed, with our potential parametrization we obtain a fairly good agreement between the absolute values of the computed and the measured heat of immersion of TiO_2 crystals as well as of the maximum adhesion force of single Tyr molecules to Ti surfaces. The latter has been obtained by means of steered MD simulations, using a time-dependent harmonic spring potential to pull the Tyr side chain off the surface. The average of the force peaks, 108 ± 31 pN, is in good agreement with the only available measured value of 97 ± 28 pN, and the computed and measured distributions present a similar standard deviation.

As far as the heat of immersion of TiO_2 is concerned, we have found a linear decrease with increasing water content chemisorbed on the surface prior to immersion in liquid water. This is consistent with the experimental study of ref 50, in which the reported range of energy values agrees very well with the simulation results. However, as already mentioned, the slope of $\Delta H_{imm}(N_{ads})$ is significantly smaller than the correspondent experimental value, probably because of dissociative adsorption events which may take place over the surface of powder crystals samples but cannot be explicitly taken into account in our classical model.

In fact, a potential as simple as the one presented here (based on purely electrostatic and LJ interactions) is expected to be accurate only under the assumption that no bond breaking or forming events take place, except the direct binding of O or N atoms of organic molecules to Ti atoms of the surface, for which the potential has been parametrized ad hoc. Under this assumption, the transferability of our potential to the case of generic organic molecules on the oxidized titanium surface is surprisingly good and allows us for the first time to investigate the atomistic mechanisms of biomolecular adsorption at titanium/water interfaces.

As a preliminary example, we have studied the adsorption of solvated RGD tripeptides on the oxidized Ti(0001) surface. Considering one possible adsorption mode, where the Arg side chain adsorbs at the surface via hydrogen bonds, we have found a free energy of desorption of 0.32 eV. The corresponding maximum detachment force reaches a value of 215 pN. As mentioned in previous publications,[14,15,58] several adsorption modes involving different side chains are possible on titanium oxide surfaces. In the context of this investigation we have restricted ourselves to just one initial configuration, in order to demonstrate the applicability of

the force field. A thorough investigation of the adsorption behavior and the corresponding free energies of RGD-containing peptides will be the subject of future work.

Future work will also be concerned with the application of the potential to larger biomolecules, which are relevant in cell adhesion processes. As already pointed out in this work, one of the main challenges in this kind of simulation will be the calculation of adsorption free energies, which becomes increasingly difficult for more complex systems. Furthermore, a possible extension of the model would be to take into account surface defects and dissociative water adsorption. However, we feel that the best way to proceed further in this direction is to implement our simple force field in hybrid QM/MM simulation schemes, such as, e.g., the Learn on the fly (LOTF) method.[65] This would enable a quantum mechanical treatment of the chemically active system regions, e.g., at the solid/liquid interface, while allowing at the same time the inclusion of a realistically large model of the physiological environment.

Acknowledgment. We acknowledge funding from the Deutsche Forschungsgemeinschaft (DFG) under the Emmy Noether grant CI 144/2-1 and from the EU-FP7-NMP grant 229205 "ADGLASS". Computer time was allocated at the HLRN (Hannover-Berlin) and the ZIH (Dresden) supercomputing centers.

Supporting Information Available: Structures and charges of the oxidized titanium surface and of the TiO_2 rutile 110 surface as well as the partial charges for the adsorbate molecules (if not taken from the AMBER force field) are available. This material is available free of charge via the Internet at http://pubs.acs.org.

References

(1) Takemoto, S.; Hattori, M.; Yoshinari, M.; Kawada, E.; Oda, Y. *Biomaterials* **2005**, *26*, 6014–6023.

(2) Aziz-Kerrzo, M.; Konroy, K. G.; Fenelon, A. M.; Farrell, S. T.; Breslin, C. B. *Biomaterials* **2001**, *22*, 1531–1539.

(3) Horbett, T. A.; Brash, J. L. In *Proteins at Interfaces II*; Horbett, T. A., Brash, J. L., Eds.; ACS Symposium Series: Washington, DC, 1995; Chapter 1, pp 1−23.

(4) Oviedo, C. *J. Phys.: Condens. Matter* **1993**, *5*, 153–154.

(5) Takakuwa, Y.; Ishidzuka, S.; Yoshigoe, A.; Teraoka, Y.; Yamamauchi, Y.; Minzuno, Y.; Tonda, H.; Homma, T. *Appl. Surf. Sci.* **2003**, *216*, 395–401.

(6) Burrell, M. C. *J. Vac. Sci. Technol., A* **1983**, *1*, 1831–1936.

(7) Liu, S.-Y.; Wang, F.-H.; Yun-Song-Zhou; Shang, J.-X. *J. Phys.: Condens. Matter* **2007**, *19*, 226004–226015.

(8) Azoulay, A.; Shamir, N.; Fromm, E.; Mintz, M. H. *Surf. Sci.* **1997**, *370*, 1–16.

(9) Vaquila, I.; Passeggi, M. C. G.; Ferron, J. *Appl. Surf. Sci.* **1996**, *93*, 247–253.

(10) Köppen, S.; Ohler, B.; Langel, W. *Z. Phys. Chem.* **2006**, *221*, 3–20.

(11) Köppen, S.; Langel, W. *Phys. Chem. Chem. Phys.* **2008**, *10*, 1907–1915.

(12) Carravetta, V.; Monti, S. *J. Phys. Chem. B* **2006**, *110*, 6160–6169.

(13) Skelton, A. A.; Liang, T.; Walsh, T. *ACS Appl. Mater. Interfaces* **2009**, *1*, 1482–1491.

(14) Liang, Y.-C.; Song, D.-P.; Chen, M.-J.; Bai, Q.-S. *J. Vac. Sci. Technol., B* **2009**, *27*, 1548–1554.

(15) Wu, C.; Chen, M.; Guo, C.; Zhao, X.; Yuan, C. *J. Phys. Chem. B* **2010**, *114*, 4692–4701.

(16) Schneider, J.; Colombi Ciacchi, L. *Surf. Sci.* **2010**, *604*, 1105–1115.

(17) Li, W.-K.; Lu, G.; Selloni, A. *J. Phys. Chem. C* **2008**, *112*, 6594–6596.

(18) Lindan, P. J. D.; Zhang, C. *Phys. Rev. B: Condens. Matter Mater. Phys.* **2005**, *72*, 075439−075445.

(19) Köppen, S.; Langel, W. *Surf. Sci.* **2006**, *600*, 2040–2050.

(20) Bandura, A. V.; Kubicki, J. D. *J. Phys. Chem. B* **2003**, *107*, 11072–11081.

(21) Skelton, A. A.; Walsh, T. *Mol. Simul.* **2007**, *33*, 379–389.

(22) Perdew, J. P.; Wang, Y. *Phys. Rev. B: Condens. Matter Mater. Phys.* **1992**, *45*, 13244–13249.

(23) Blöchl, P. E. *Phys. Rev. B: Condens. Matter Mater. Phys.* **1994**, *50*, 17953–17979.

(24) Vita, A. D.; Canning, A.; Galli, G.; Gygi, F.; Mauri, F.; Car, R. *EPFL Supercomput. Rev.* **1994**, *6*, 22.

(25) Car, R.; Parrinello, M. *Phys. Rev. Lett.* **1985**, *55*, 2471–2474.

(26) VandeVondele, J.; Vita, A. D. *Phys. Rev. B: Condens. Matter Mater. Phys.* **1999**, *60*, 13241–13244.

(27) Stengel, M.; Vita, A. D. *Phys. Rev. B: Condens. Matter Mater. Phys.* **2000**, *62*, 15283–15286.

(28) Neugebauer, J.; Scheffler, M. *Phys. Rev. B: Condens. Matter Mater. Phys.* **1992**, *46*, 16067–16080.

(29) Todorov, I. T.; Smith, W. *Phil. Trans. R. Soc., A* **2004**, *362*, 1835–1852.

(30) Berendsen, H. J. C.; Postma, J. P. M.; van Gunsteren, W.; DiNola, A.; Haak, J. R. *J. Chem. Phys.* **1984**, *81*, 3684–3690.

(31) Langel, W. *Surf. Sci.* **2002**, *496*, 141–150.

(32) Barnard, A. S.; Zapol, P.; Curtiss, L. A. *Surf. Sci.* **2005**, *582*, 173–188.

(33) Diebold, U. *Surf. Sci. Rep.* **2003**, *48*, 53–229.

(34) Henderson, M. A. *Surf. Sci.* **1996**, *355*, 151–166.

(35) Wendt, S.; Matthiesen, J.; Schaub, R.; Vestergaard, E. K.; Lægsgaard, E.; Besenbacher, F.; Hammer, B. *Phys. Rev. Lett.* **2006**, *96*, 066107−066110.

(36) Cheng, J.; Sprik, M. *J. Chem. Theory Comput.* **2010**, *6*, 880–889.

(37) Zimmermann, J.; Finnis, M. W.; Colombi Ciacchi, L. *J. Chem. Phys.* **2009**, *130*, 134714–134725.

(38) Lausmaa, J.; Loefgren, P.; Kasemo, B. *J. Biomed. Mater. Res.* **1999**, *44*, 227–242.

(39) Mortier, W. J.; Genechten, K. V.; Gasteiger, J. *J. Am. Chem. Soc.* **1985**, *107*, 829–835.

(40) Bader, R. F. W. In *Atoms in Molecules: A Quantum Theory*; Oxford University Press: Oxford, U.K., 1994; Chapter 6, pp 169−247.

(41) Jorgensen, W. L.; Chandrasekhar, J.; Madura, J. D.; Impey, R. W.; Klein, M. L. *J. Chem. Phys.* **1983**, *79*, 926–935.

(42) Cornell, W. D.; Cieplak, P.; Bayly, C. I.; Gould, I. R.; Merz Jr, K. M.; Ferguson, D. M.; Spellmeyer, D. C.; Fox, T.;

Caldwell, J. W.; Kollman, P. A. *J. Am. Chem. Soc.* **1995**, *117*, 5179–5197.

(43) Momany, F. A. *J. Phys. Chem.* **1978**, *82*, 592–601.

(44) Cox, S. R.; Williams, D. E. *J. Comput. Chem.* **1981**, *2*, 304–323.

(45) Singh, U. C.; Kollman, P. A. *J. Comput. Chem.* **1984**, *5*, 129–145.

(46) Woods, R. J.; Khalil, M.; Pell, W.; Moffat, S. H.; Smith, V. H., Jr. *J. Comput. Chem.* **1990**, *11*, 297–310.

(47) Wang, J.; Wolf, R. M.; Caldwell, J. W.; Kollman, P. A.; Case, D. A. *J. Comput. Chem.* **2004**, *25*, 1157–1174.

(48) Gale, J. D. *J. Chem. Soc., Faraday Trans.* **1997**, *93*, 629–637.

(49) Ortmann, F.; Schmidt, W. G.; Bechstedt, F. *Phys. Rev. Lett.* **2005**, *95*, 186101–186104.

(50) Morimoto, T.; Nagao, M.; Omori, T. *Bull. Chem. Soc. Jpn.* **1969**, *42*, 943–946.

(51) Gun'ko, V. M.; Blitz, J. P.; Zarko, V. I.; Turov, V. V.; Pakhlov, E. M.; Oranska, O. I.; Goncharuk, E. V.; Gornikov, Y. I.; Sergeev, V. S.; Kulik, T. V.; Palyanytsya, B. B.; Samala, R. K. *J. Colloid Interface Sci.* **2009**, *330*, 125–137.

(52) Dawber, J. G.; Guest, L. B.; Lambourne, R. *Thermochim. Acta* **1972**, *4*, 471–484.

(53) Cole, D. J.; Csanyi, G.; Payne, M. C.; Spearing, S. M.; Colombi Ciacchi, L. *J. Chem. Phys.* **2007**, *127*, 204704–204715.

(54) Lee, H.; Scherer, N. F.; Messersmith, P. B. *Proc. Natl. Acad. Sci. U.S.A.* **2006**, *103*, 12999–13003.

(55) Ruoslahti, E.; Pierschbacher, M. D. *Science* **1987**, *238*, 491–497.

(56) Xiao, S.-J.; Textor, M.; Spencer, N. D. *Langmuir* **2998**, *14*, 5507–5516.

(57) Rammelt, S.; Illert, T.; Bierbaum, S.; Scharnweber, D.; Zwipp, H.; Schneiders, W. *Biomaterials* **2006**, *27*, 5561–5571.

(58) Song, D.-P.; Chen, M.-J.; Liang, Y.-C.; Bai, Q.-S.; Chen, J.-X.; Zheng, X.-F. *Acta Biomat.* **2010**, *6*, 684–694.

(59) Kumar, S.; Bouzida, D.; Swendsen, R. H.; Kollman, P. A.; Rosenberg, J. M. *J. Comput. Chem.* **1992**, *13*, 1011–1021.

(60) Grossfield, A. *WHAM: The weighted histogram analysis method*; University of Rochester Medical Center: Rochester, NY; http://membrane.urmc.rochester.edu/content/wham. Accessed August 17, 2009.

(61) Darve, E. In *Free Energy Calculations*; Chipot, C., Pohorille, A., Eds.; Springer, Berlin, Germany, 2007; Chapter 4, pp 119−170.

(62) Trzesniak, D.; Kunz, A.-P. E.; van Gunsteren, W. F. *Chem. Phys. Chem.* **2007**, *8*, 162–169.

(63) Lee, I.; Marchant, R. *Surf. Sci.* **2001**, *491*, 433–443.

(64) Choi, Y.; Kim, E.; Lee, Y.; Han, M. H.; Kang, I.-C. *Proteomics* **2010**, *10*, 72–80.

(65) Csanyi, G.; Albaret, T.; Payne, M. C.; Vita, A. D. *Phys. Rev. Lett.* **2004**, *93*, 175503–175506.

CT1004388